Catalysis Today 146 (2009) 31–36

Contents lists available at ScienceDirect

Catalysis Today

journal homepage: www.elsevier.com/locate/cattod

Ethanol steam reforming over Ni and Ni–Cu catalysts

Fagen Wang, Yong Li, Weijie Cai, Ensheng Zhan, Xiaoling Mu, Wenjie Shen *

State Key Laboratory of Catalysis, Dalian Institute of Chemical Physics, Chinese Academy of Sciences, 457 Zhongshan Road, Dalian 116023, China

ARTICLE INFO

Article history:
Available online 8 February 2009

Keywords:
Ethanol
Steam reforming
Hydrogen
Ni catalysts
Deactivation

ABSTRACT

Steam reforming of ethanol over unsupported Ni and Ni–Cu catalysts was investigated. Ethanol and the reaction intermediates like acetaldehyde and acetone are entirely converted into hydrogen and C_1 products at 400 °C, while methane steam reforming and reversible water gas shift are the major reactions at higher temperatures. The Ni–Cu catalyst exhibited stable performance during 40 h on-stream at 650 °C without apparent deactivation, but the Ni catalyst showed severe deactivation only after 12 h on-stream due to heavy coke deposition. Filament carbon was mainly produced on the Ni catalyst through the Boudouard reaction, whereas condensed carbon was formed on the Ni–Cu catalyst by methane decomposition.

1. Introduction

Hydrogen production by steam reforming (SR) of ethanol has recently attracted wide attention because of the increasing concern in effective utilization of bio-ethanol and the potential application in fuel cells. To date, most studies have focused on supported Ni [1–4], Co [5–7], Ir [8], and Rh [9] catalysts for SR of ethanol, operated at relative higher temperatures, typically 600–800 °C. Among them, Ir and Rh catalysts show the most effective and promising performance with respect to ethanol conversion and hydrogen productivity. However, the high cost of noble metals limits their practical applications.

Among the non-precious metals, Ni catalyst is the most favorable candidate in SR of ethanol, which exhibits adequate activity through the strong capability of breaking the C–C bond in ethanol, but it usually results in low-hydrogen yield because of the formation of significant amounts of methane [1–4,10]. Meanwhile, the Ni catalyst also suffers sever deactivation caused by the sintering Ni particle and the heavy coke deposition during the course of reaction. The sintering of Ni particle rapidly decreases the activity, but it can be partially inhibited by using additional metals such as Ag [11], Rh [12], and Cu [13–15] through the formation of metal alloys. For example, the combination of Ni and Cu showed higher activity and longer stability for SR of ethanol. The formation of Ni–Cu alloy resulted in the preferential elimination of large Ni ensembles necessary for carbon deposition [14]. On the other hand, coke deposition is the major reason for the deactivation of Ni catalysts during ethanol SR [3,4,10]. The Ni catalysts reported so far for ethanol SR use metal oxides as supports to disperse the fine Ni particles and to prevent their sintering under reaction conditions. But the acidic and/or basic nature of the metal oxides usually favors the dehydration of ethanol to ethylene and its oligomerization [4,10], which is largely contributed to the formation of carbon in ethanol SR. Reforming of methane, formed by the decomposition of ethanol, also produced significant amounts of carbon, especially at temperatures above 400 °C [16,17]. Additionally, the Boudouard reaction that is thermodynamically favored below 700 °C may convert the produced CO into carbon as well [18]. Although not all of the deposited carbon causes the loss of activity, like filamentous carbon [10], it is generally acknowledged that the encapsulating carbon would cause significant deactivation. Therefore, it seems that carbon deposition is still the major difficulty to develop the long-term stable and coke resistant Ni catalysts.

We have previously reported that unsupported fibrous nickel is very active for methane decomposition to produce hydrogen and carbon nanofiber [19]. In this work, we examined these Ni and Ni–Cu catalysts for ethanol steam reforming where the formation of coke through ethylene was eliminated due to the absence of acidic or basic metal oxides [4,10]. The catalytic stabilities of the Ni and Ni–Cu catalysts for ethanol SR were comparatively studied and the coke depositions during the courses of reaction were extensively analyzed.

2. Experimental

2.1. Catalyst preparation

The nickel hydroxide was prepared by precipitation of nickel acetate dissolved in ethylene glycol with sodium carbonate aqueous solution at 120 °C, as described elsewhere [19]. A mixture

* Corresponding author. Tel.: +86 411 84379085; fax: +86 411 84694447.
E-mail address: shen98@dicp.ac.cn (W. Shen).

0920-5861/$ – see front matter © 2009 Elsevier B.V. All rights reserved.
doi:10.1016/j.cattod.2009.01.027

containing 0.05 mol of nickel acetate ($Ni(OAc)_2{\cdot}4H_2O$) and 150 ml of ethylene glycol (EG) was heated to 120 °C under stirring and maintained at the same temperature for 30 min. 500 ml of 0.2 M aqueous Na_2CO_3 solution were then slowly added to the Ni-EG solution with a final pH value of about 10. The precipitate was aged in the mother liquid for 1 h. After being filtered and washed thoroughly with distilled water, the nickel hydroxide precipitate was dried at 100 °C overnight and finally calcined in air at 700 °C for 6 h, giving NiO.

The $Ni_{0.99}Cu_{0.01}O$ sample was prepared with the same procedure as that of the NiO, but a mixture of nickel and copper acetates with a proper Ni/Cu ratio was used.

2.2. Catalyst characterization

N_2 adsorption–desorption isotherms were recorded at −196 °C using ASAP V2.02 instrument. Before the measurement, the sample was degassed at 300 °C for 2 h. The surface area of the sample was calculated by a multipoint Braunauer–Emmett–Teller (BET) analysis of the nitrogen adsorption isotherm.

X-ray power diffraction (XRD) patterns were recorded using a Rigaku D/MAX-RB diffractor with a Ni-filtered Cu Kα radiation operated at 40 kV and 200 mA. The spectra were taken in the 2θ range of 10–80° at a scan speed of 5°/min with a step interval of 0.02°. In situ XRD measurements for the reductions of the NiO and $Ni_{0.99}Cu_{0.01}O$ samples were performed in a high-temperature chamber. The sample was heated 650 °C under N_2 flow, and a 5 vol% H_2/N_2 mixture was introduced into the chamber and kept at 650 °C for 3 h, after which the XRD patterns were recorded. The mean crystalline sizes of NiO and Ni were calculated according to the Scherrer equation.

Transmission electron microscopy (TEM) images were taken on Philips Tecnai G^2 Spirit microscope operated at 120 kV. Specimens were prepared by ultrasonically suspending the sample in ethanol. A drop of the suspension was deposited on a thin carbon film supported on a standard copper grid and dried in air.

Temperature-programmed reduction (TPR) measurement was performed with a conventional setup equipped with a thermal conductivity detector. 50 mg (40–60 mesh) samples were pretreated at 300 °C for 1 h under N_2 flow (40 ml/min). After cooling to room temperature and introducing the reduction agent of a 5 vol% H_2/N_2 mixture (40 ml/min), the temperature was then programmed to 700 °C at a rate of 10 °C/min.

Temperature-programmed hydrogenation (TPH) and oxidation (TPO) of the deposited carbon on the catalyst were performed in U-type quartz tubular reactor equipped with a mass spectrometer. 20 mg of the used catalysts were loaded and the sample was heated from room temperature to 700 °C at a rate of 10 °C/min under the flow of a 20 vol% H_2/He mixture (30 ml/min for TPH) or a 20 vol% O_2/He mixture (30 ml/min for TPO). The m/e intensities of 16 (CH_4), 18 (H_2O), 28 (CO), 28 (C_2H_4), 30 (C_2H_6), and 44 (CO_2) were monitored by the mass spectrometer. The amount of carbon deposited on the catalyst was calculated according to the intensities of carbon oxides.

2.3. Catalytic evaluation

Ethanol steam reforming was conducted in a continuous-flow fixed bed quartz reactor at atmospheric pressure. 100 mg of catalyst (40–60 mesh) was loaded and sandwiched by two layers of quartz wool. Before the reaction, the catalyst was reduced with a 5 vol% H_2/He (20 ml/min) mixture at 650 °C for 3 h. Then, the temperature was set to 400–650 °C under N_2 flow and a 50 vol% ethanol aqueous solution (water/ethanol molar ratio of 3/1) was fed by a micro-pump with a gas hourly space velocity (GHSV) of 6000 ml/g h. The effluent was analyzed by on-line gas chromatography equipped with a thermal conductivity detector and a flame ionization detector. The concentrations of the products were calculated by excluding water, that is, dry-based gas composition. The reaction test at each temperature was conducted for 10 h, during which no obvious deactivation was detected and the average conversion of ethanol and the mean composition of the product were used.

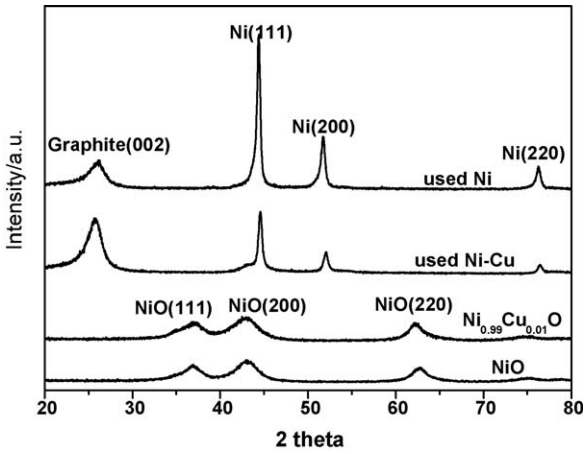

Fig. 1. XRD patterns of the NiO and $Ni_{0.99}Cu_{0.01}O$ samples and the used Ni and Ni–Cu catalysts for ethanol steam reforming.

3. Results and discussion

3.1. Physical and chemical properties of the Ni catalysts

Fig. 1 shows the XRD patterns of the NiO and $Ni_{0.99}Cu_{0.01}O$ samples. Only the diffraction peaks of nickel oxide with cubic structure (JCPDS# 4-835) were observed, and the average crystalline sizes of NiO were about 4 nm in both cases. There were no diffraction peaks of CuO in the $Ni_{0.99}Cu_{0.01}O$ sample probably because of the very low content. Fig. 2 shows the TEM images of the two samples. Clearly, the nickel oxides exhibited inter-layered structure, and the addition of copper oxide did not alter the fibrous shape of the NiO. The specific surface areas of the NiO and $Ni_{0.99}Cu_{0.01}O$ samples were 126 and 129 m^2/g, respectively.

Fig. 3 shows the H_2-TPR profiles of the oxides. The reduction of NiO occurred at about 700 °C with a small shoulder at 320 °C, character of fibrous nickel oxide [19]. The $Ni_{0.99}Cu_{0.01}O$ sample exhibited two hydrogen consumptions at 360 and 700 °C, respectively. The former is due to the reduction of copper oxide, which probably has a strong interaction with nickel oxide [20], while the latter is attributed to the reduction of nickel oxide. This implies that the addition of small amounts of copper oxide does not appreciably change the reduction feature of the fibrous nickel oxide.

Fig. 4 illustrates the XRD patterns of the Ni catalysts obtained by reducing the NiO and $Ni_{0.99}Cu_{0.01}O$ samples with hydrogen at 650 °C. Both NiO and $Ni_{0.99}Cu_{0.01}O$ were fully reduced to metallic nickel with a similar crystallite size of 11 nm. There were no diffraction peaks of copper mainly due to the very low content and the possible formation of Ni–Co alloy. This phenomenon is accord with the observation in the TPR profiles that the presence of copper oxide does not apparently modify the reduction feature of the fibrous nickel oxide.

3.2. Steam reforming of ethanol

Fig. 5 shows the temperature dependence of the product distribution during ethanol steam reforming over the Ni and Ni–

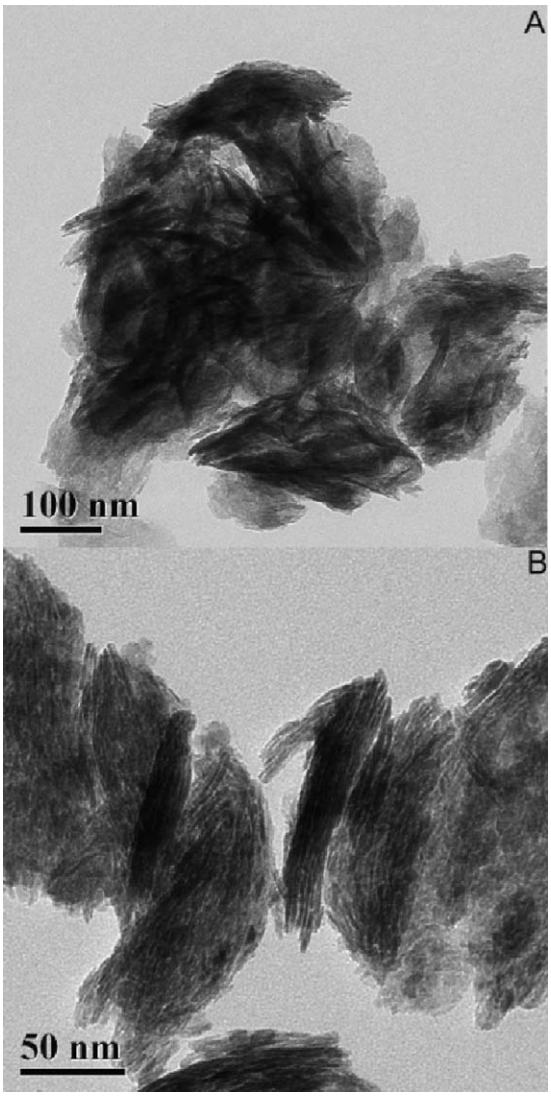

Fig. 2. TEM images of the NiO (A) and $Ni_{0.99}Cu_{0.01}O$ (B) samples.

Cu catalysts. Ethanol and the reaction intermediates like acetaldehyde and acetone was entirely converted to hydrogen and C_1 products at 400 °C, indicating the high activity of the Ni catalysts because most supported Ni catalysts could give ~100% ethanol conversion only above 500 °C [3,4,21–23]. The concentration of hydrogen increased progressively with temperature, whereas the concentration of CH_4 and CO_2 decreased gradually. This suggests that steam reforming of methane and reverse water gas shift (WGS) reactions, which are thermodynamically feasible, occur as the major reactions. At 650 °C, methane was almost completely reformed, while the concentration of CO slightly increased due to the equilibrium limit of the WGS reaction. The

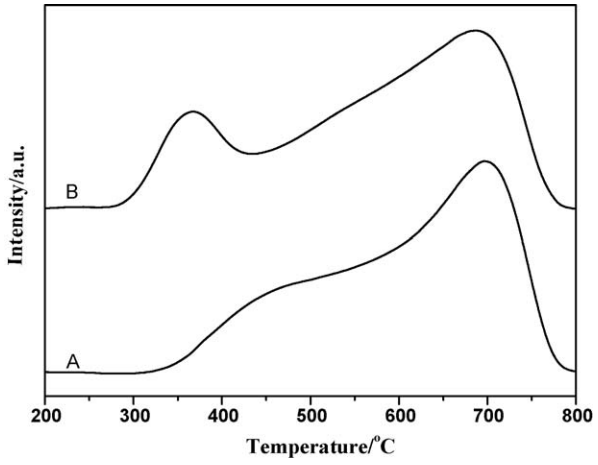

Fig. 3. TPR profiles of the NiO (A) and $Ni_{0.99}Cu_{0.01}O$ (B) samples.

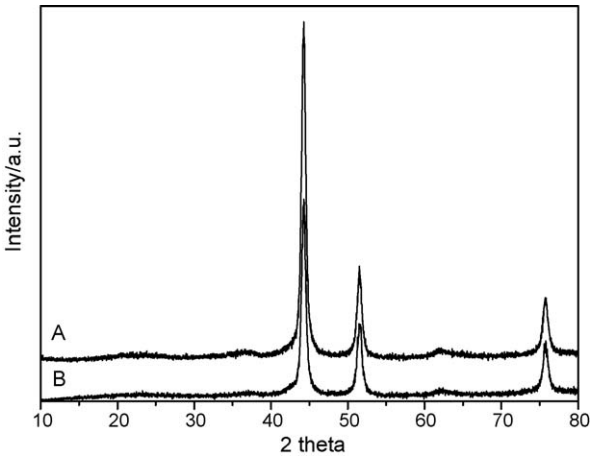

Fig. 4. XRD patterns of the Ni (A) and Ni–Cu (B) catalysts.

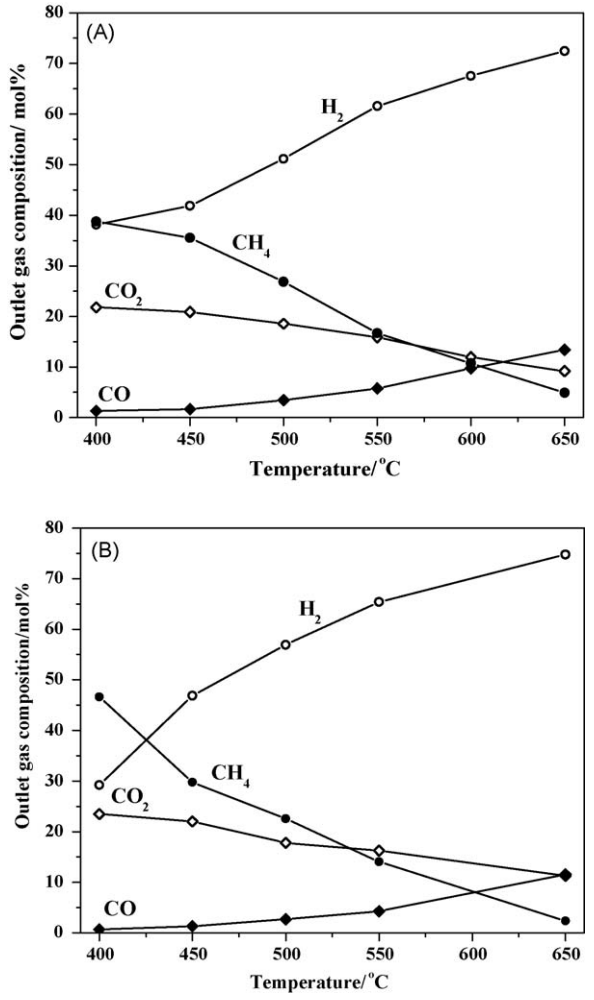

Fig. 5. Effect of reaction temperature on the product distribution for steam reforming of ethanol over the Ni (A) and Ni–Cu (B) catalysts. Reaction conditions: C_2H_5OH/H_2O = 1:3 (molar ratio), GHSV = 6000 ml/g h.

very similar reaction patterns between the Ni and the Ni–Cu catalysts confirm that the addition of copper does not change the product distribution of ethanol steam reforming in the temperature range examined. It has been reported that the addition of copper (2%) to a 7% Ni/SBA-15 catalyst could promote the WGS reaction, especially at lower temperatures [15]. However, such a promotional effect is not observed for the present Ni–Cu catalyst, probably because of the very low-copper content (1%) and the sufficient activity of Ni for SR of ethanol.

Fig. 6 compares the concentrations of H_2, CO, CO_2, and CH_4 in the outlet streams as a function of time-on-stream at 650 °C over the Ni and Ni–Cu catalysts. The Ni catalyst showed relatively stable performance at the initial 8 h, and then the concentration of hydrogen tended to decrease while the concentrations of CO and CH_4 increased significantly. The pressure of the reactor was also increased, indicating the occurrence of heavy coke deposition on the surface of the catalyst. In contrast, the Ni–Cu catalyst exhibited rather stable performance for 40 h on-stream without apparent variations in the concentrations of the products. This quite promising activity and stability of the fibrous Ni–Cu catalyst might be caused by the formation of Ni–Cu alloy [15]. The outlet

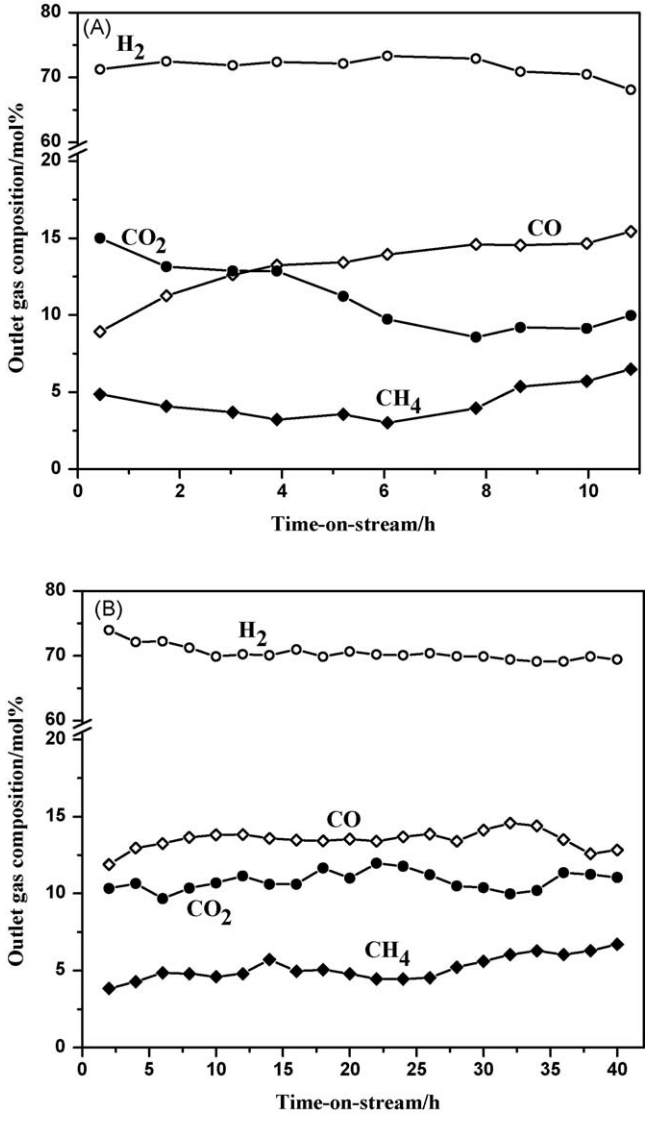

Fig. 6. Alternation of outlet gas composition for steam reforming of ethanol over the Ni (A) and Ni–Cu (B) catalysts. Reaction conditions: T = 650 °C, C_2H_5OH/H_2O = 1:3, GHSV = 6000 ml/g h.

stream consisted of 72% H_2, 13% CO, 10% CO_2, and 4% CH_4. Thermodynamic analysis for ethanol steam reforming under the current reaction conditions revealed that the equilibrium gas composition is 55% H_2, 21% CH_4, 13% CO and 11% CO_2 [24]. Apparently, the outlet gas composition of ethanol SR on the Ni–Cu catalyst is far from the thermodynamic equilibrium, particularly in the contents of hydrogen and methane. This phenomenon might be caused the high activity of fibrous Ni for methane decomposition, producing hydrogen and carbon on the surface of the catalyst [19].

3.3. Coke deposition

Fig. 1 also shows the XRD patterns of the used Ni and Ni–Cu catalysts. In addition to the typical diffraction peaks of metallic nickel, a board diffraction peak at $2\theta = 26°$ was observed, representing the deposited carbon. The crystalline size of Ni was 30 nm in the Ni catalyst after operating for 12 h, whereas the size of Ni crystallite was 45 nm in the Ni–Cu catalyst even it was operated for 40 h. Although the initial crystallite size of nickel in the two catalysts was 11 nm, the crystallite size of 45 nm in the used Ni–Cu catalyst for 40 h on-stream implies that the copper effectively prevents the nickel particles from sintering during the course of reaction, probably through the formation Ni–Cu alloy. Furthermore, a very minor diffraction peak of NiO appeared at around $2\theta = 43°$, which might be caused by the exposure to air during the sample handling or the possible oxidation of Ni under the reaction conditions.

Fig. 7 shows the TEM images of the used Ni and Ni–Cu catalysts. For the Ni catalyst, filament carbon with rough surface was formed and most of the Ni particles with size of 10–40 nm were encapsulated by the deposited carbon. In the case of the Ni–Cu catalyst, however, mainly condensed carbon was produced, which is similar to the carbon deposited on the Ni/MgO catalyst [25,26]. Most of the Ni particles having size of 20–60 nm were dispersed on the deposited carbon, instead of being encapsulated. It seems that the presence of Ni–Cu alloy inhibits the formation of encapsulating coke through the efficient hydrogen mobility of copper [14,27]. This is similar to the previous observation that the addition of copper to Ni catalysts could change the morphology of the deposited carbon by adjusting the electronic feature and the affinity with carbon of nickel particle [28].

Fig. 8 shows the TPO profiles of the used Ni and Ni–Cu catalysts. The evolution of CO_2 over the Ni catalyst occurred at a relatively lower temperature than that over the Ni–Cu catalyst, suggesting that that the carbon species deposited on the Ni catalyst is slightly reactive than that on the Ni–Cu catalyst. The total amount of deposited carbon was almost the same in both cases, 21–22 mg/g, but the deposition rate of carbon on the Ni–Cu catalyst (0.53 mg C/h) was much less than that on the Ni catalyst (1.83 mg C/h). This demonstrates that the Ni–Cu catalyst has a better resistance towards carbon deposition during the course of ethanol SR. This promotional effect has also been observed on SiO_2, SBA-15 and Al_2O_3 supported Ni–Cu catalysts, which was ascribed to the preferential elimination of larger ensembles of Ni atoms necessary for carbon deposition with the addition of copper [29].

Fig. 9 presents the TPH profiles of the used Ni and Ni–Cu catalysts. Two main evolution peaks of methane were observed at about 350 and 590 °C on the two catalysts, demonstrating that the carbon formed during the course of ethanol SR is in graphitic nature [16,17]. However, trace amounts of ethylene were also produced on the Ni–Cu catalyst. This implies that carbon deposition over the two catalysts may origin from different sources. Since the graphitic carbon formed by CO dissociation

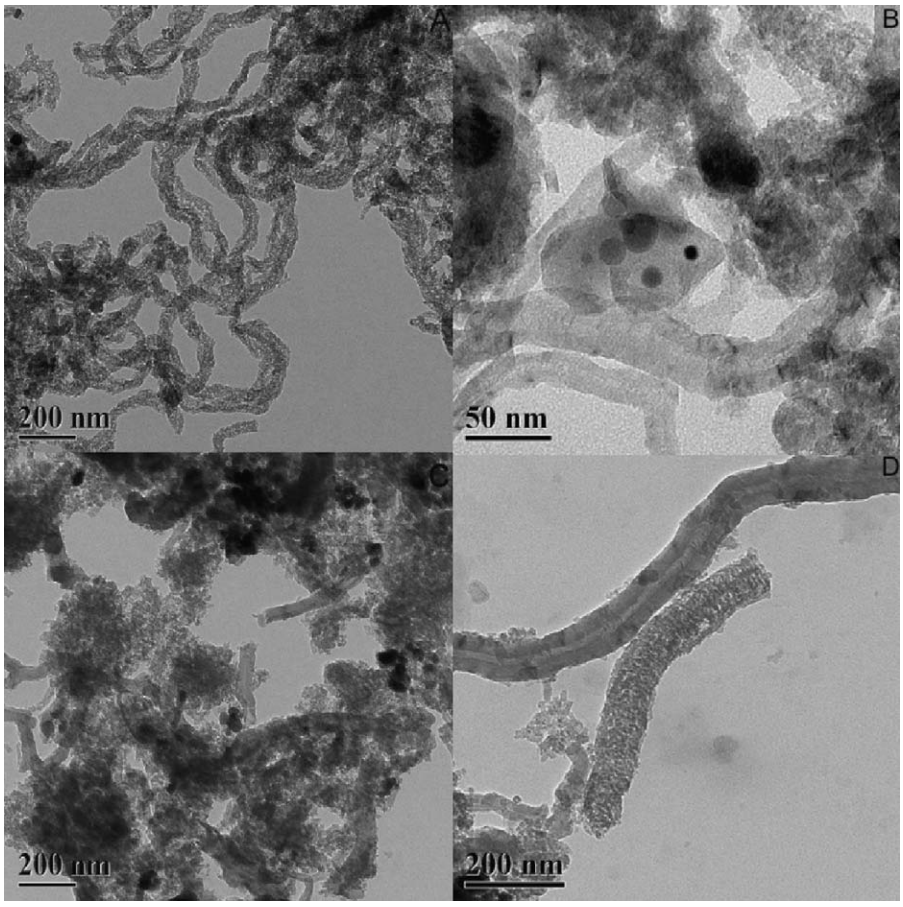

Fig. 7. TEM images of the used Ni (A and B) and Ni–Cu (C and D) catalysts.

usually tends to encapsulate the Ni particle with rough surface [27], the carbon deposited on the Ni catalyst seems to be originated from the Boudouard reaction. Whereas the carbon formed on the Ni–Cu catalyst is probably caused by the decomposition of methane.

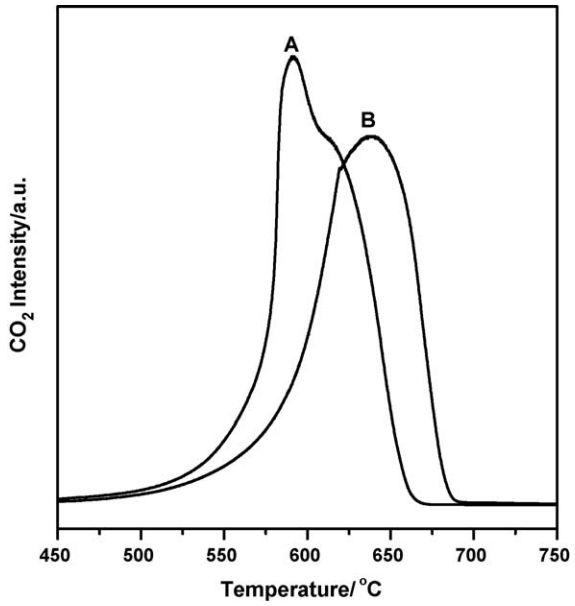

Fig. 8. TPO profiles of the used Ni (A) and Ni–Cu (B) catalysts.

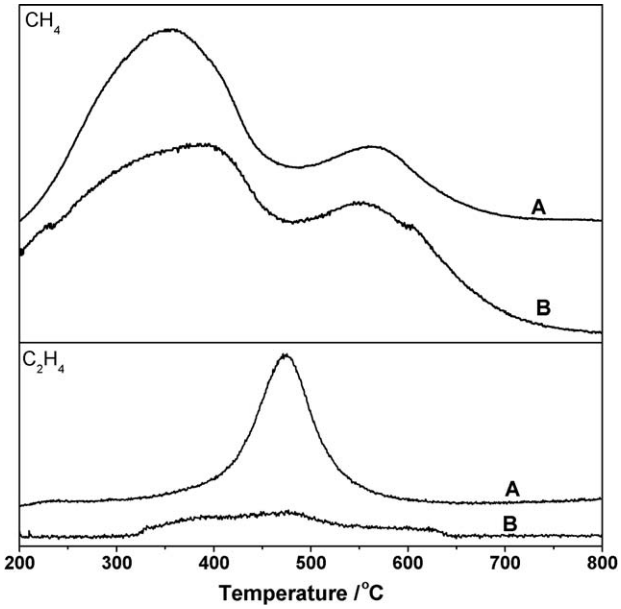

Fig. 9. TPH profiles of the used Ni (A) and Ni–Cu (B) catalysts.

4. Conclusions

The Ni–Cu catalyst was highly active and stable for steam reforming of ethanol even with a stoichiometric feed composition. Ethanol and the reaction intermediates were entirely reformed

into hydrogen and C_1 products at 400 °C, methane steam reforming and reversible water gas shift became the major reactions at higher temperatures. The Ni–Cu catalyst exhibited stable performance during 40 h on-stream at 650 °C without apparent deactivation, evidenced by the consistent composition of the outlet stream. Condensed carbon was deposited on the Ni–Cu catalyst, probably through the decomposition of methane formed during ethanol steam reforming.

Acknowledgement

We gratefully acknowledge the financial support from the National Natural Science Foundation of China (grant number 20773119).

References

[1] J.W.C. Liberatori, R.U. Ribeiro, D. Zanchet, F.B. Noronha, J.M.C. Bueno, Appl. Catal. A 327 (2007) 197.
[2] F. Frusteri, S. Freni, J. Power Sources 173 (2007) 200.
[3] M. Ni, D.Y.C. Leung, M.K.H. Leung, Int. J. Hydrogen Energy 32 (2007) 3238.
[4] A.N. Fatsikostas, X.E. Verykios, J. Catal. 225 (2004) 439.
[5] J. Llorca, N. Homs, J. Sales, P. Ramírez de la Piscina, J. Catal. 209 (2002) 306.
[6] M.S. Batista, R.K.S. Santos, E.M. Assaf, J.M. Assaf, E.A. Ticianelli, J. Power Sources 134 (2004) 27.
[7] S. Tuti, F. Pepe, Catal. Lett. 122 (2008) 196.
[8] W.J. Cai, F.G. Wang, E.S. Zhan, A.C. Van Veen, C. Mirodatos, W.J. Shen, J. Catal. 257 (2008) 96.
[9] G.A. Deluga, J.R. Salge, L.D. Schmidt, X.E. Veryios, Science 303 (2004) 993.
[10] A.L. Alberton, M.M.V.M. Souza, M. Schmal, Catal. Today 123 (2007) 257.
[11] N.V. Parizotto, K.O. Rocha, S. Damyanova, F.B. Passos, D. Zanchet, C.M.P. Marques, J.M.C. Bueno, Appl. Catal. A 330 (2007) 12.
[12] J. Kugai, V. Subramani, C. Song, M.H. Engelhard, Y.H. Chin, J. Catal. 238 (2006) 430.
[13] F. Marino, M. Boveri, G. Baronetti, M. Laborde, Int. J. Hydrogen Energy 29 (2004) 67.
[14] A.J. Vizcaíno, A. Carrero, J.A. Calles, Int. J. Hydrogen Energy 32 (2007) 1450.
[15] A. Carrero, J.A. Calles, A.J. Vizcaíno, Appl. Catal. A 327 (2007) 82.
[16] C.H. Bartholomew, Appl. Catal. A 212 (2001) 17.
[17] Y.H. Hu, E. Ruckenstein, Adv. Catal. 48 (2004) 297.
[18] J.R. Rostrup-Nielsen, Adv. Catal. 47 (2002) 65.
[19] Y. Li, B.C. Zhang, X.W. Xie, J.L. Liu, Y.D. Xu, W.J. Shen, J. Catal. 238 (2006) 412.
[20] L. Dussault, J.C. Dupin, C. Guimon, M. Monthioux, N. Latorre, T. Ubieto, E. Romeo, C. Royo, A. Monzón, J. Catal. 251 (2007) 223.
[21] S. Freni, S. Cavallaro, N. Mondello, L. Spadaro, F. Frusteri, Catal. Commun. 4 (2003) 259.
[22] Y. Yang, J. Ma, F. Wu, Int. J. Hydrogen Energy 31 (2006) 877.
[23] P. Biswas, D. Kunzru, Chem. Eng. J. 36 (2008) 41.
[24] Fishtik, A. Alexander, R. Datta, D. Geana, Int. J. Hydrogen Energy 25 (2001) 31.
[25] F. Frusteri, S. Freni, V. Chiodo, L. Spadaro, O. Di Blasi, G. Bonura, S. Cavallaro, Appl. Catal. A 270 (2004) 1.
[26] F. Frusteri, S. Freni, V. Chiodo, L. Spadaro, G. Bonura, S. Cavallaro, J. Power Sources 132 (2004) 39.
[27] Y. Nishiyama, Y. Tamai, J. Catal. 33 (1974) 98.
[28] J.L. Chen, Y.D. Li, Y.M. Ma, Y.N. Qin, L. Chang, Carbon 39 (2001) 1467.
[29] H.W. Chen, C.Y. Wang, L.T. Tseng, P.H. Liao, Catal. Today 97 (2004) 173.